crystals

MDPI

Article

Effect of Bi^{3+} Doping on the Electronic Structure and Thermoelectric Properties of $(Sr_{0.889-x}La_{0.111}Bi_x)TiO_{2.963}$: First-Principles Calculations

Lingyun Gong [1], Ping Zhang [1], Zhihao Lou [1], Ziyao Wei [1], Zhuozhao Wu [2], Jie Xu [1], Xuanjie Chen [2], Weihang Xu [2], Yiqi Wang [2] and Feng Gao [1,*]

[1] State Key Laboratory of Solidification Processing, MIIT Key Laboratory of Radiation Detection Materials and Devices, NPU-QMUL Joint Research Institute of Advanced Materials and Structure, USI Institute of Intelligence Materials and Structure, School of Materials Science and Engineering, Northwestern Polytechnical University, Xi'an 710072, China

[2] Queen Mary University of London Engineering School, Northwestern Polytechnical University, Xi'an 710072, China

* Correspondence: gaofeng@nwpu.edu.cn

Abstract: The electronic structure and thermoelectric properties of Bi^{3+}-doped $(Sr_{0.889-x}La_{0.111}Bi_x)TiO_{2.963}$ were studied by the first principles method. Doping Bi^{3+} can increase the cell parameters, cell asymmetry and band gap. With increasing Bi^{3+} content, the asymmetry of DOS relative to the Fermi level increases, which results in an enhanced Seebeck coefficient, increasing carrier mobility and decreasing carrier concentration. An appropriate Bi^{3+}-doping concentration (7.4–14.8%) can increase the lattice distortion and reduce the lattice thermal conductivity of the material. An appropriate Bi^{3+}-doping concentration (7.4%) can effectively optimize the electrical transport performance and improve the thermoelectric properties of strontium titanate. The optimal Bi^{3+}-doping concentration is 7.4%, and $Sr_{0.815}La_{0.111}Bi_{0.074}TiO_{2.963}$ obtains a maximum ZT of 0.48. This work shows the mechanism of Bi^{3+} doping in enhancing the thermoelectric properties of strontium titanate.

Keywords: thermoelectric properties; first principles; solid-state reaction method; cation doping

check for updates

Citation: Gong, L.; Zhang, P.; Lou, Z.; Wei, Z.; Wu, Z.; Xu, J.; Chen, X.; Xu, W.; Wang, Y.; Gao, F. Effect of Bi^{3+} Doping on the Electronic Structure and Thermoelectric Properties of $(Sr_{0.889-x}La_{0.111}Bi_x)TiO_{2.963}$: First-Principles Calculations. *Crystals* **2023**, *13*, 178. https://doi.org/10.3390/cryst13020178

Academic Editor: Andrei Vladimirovich Shevelkov

Received: 31 December 2022
Revised: 15 January 2023
Accepted: 16 January 2023
Published: 19 January 2023

Copyright: © 2023 by the authors. Licensee MDPI, Basel, Switzerland. This article is an open access article distributed under the terms and conditions of the Creative Commons Attribution (CC BY) license (https://creativecommons.org/licenses/by/4.0/).

1. Introduction

Due to environmental pollution and other problems, researchers around the world are actively looking for new energy materials for sustainable development. Thermoelectric materials can directly convert heat into electricity through the Seebeck effect [1], and can be widely used in automobiles, refrigeration, space and other fields [2]. Thermoelectric superior value ($ZT = S^2 \times \sigma \times T/\kappa$) is generally used to evaluate the performance of thermoelectric materials. Through the application of thermoelectric materials with high ZT values, waste heat recovery can be realized to improve energy utilization efficiency.

Strontium titanate ($SrTiO_3$, STO) is a typical *n*-type oxide thermoelectric material with a cubic perovskite structure, good thermal stability and broad application prospects. However, the ZT value of strontium titanate is low and cannot meet the application requirements. Therefore, researchers have conducted a lot of studies on $SrTiO_3$ to improve its thermoelectric properties, such as doping modification [3], grain boundary engineering [4], composite second phase [5], etc. Among them, La^{3+}-doping $SrTiO_3$ [4–12] has been extensively studied and achieved good results. On the basis of the thermoelectric properties of La^{3+}-doping $SrTiO_3$, it is a difficult problem to further improve the thermoelectric properties of the material.

In addition to experimental research, many scholars have also carried out theoretical calculation research on $SrTiO_3$ materials. In particular, the electronic structure and physical properties of the intrinsic [13,14] and doped [15–24] $SrTiO_3$ material have been calculated using first principles. Singsoog [17] constructed a supercell containing four protocells and

studied the electronic structure and electrical transport properties of $Sr_{1-x}La_xTiO_3$(x = 0, 0.06, 0.13 and 0.25) based on first-principles molecular orbital calculations. $Sr_{0.87}La_{0.13}TiO_3$ shows a maximum power factor of about 2.55 × 10^{-3}W/(m·K^2) at 1200 K. Baniecki20 constructed $Sr_{1-x}La_xTiO_3$ and $SrTi_{1-x}M_xO_3$(M = V, Nb, Ta)(x = 0.125) containing eight protocells, and systematically studied the changes in electronic structure, carrier effective mass, splitting energy and transport characteristics caused by doping.

According to current research, doping tends to change the electronic structure of materials to enhance the *S* of materials, while heavy ion doping tends to enhance phonon scattering and reduce the lattice thermal conductivity of materials. In the power factor ($PF = S^2\sigma$) where *S* is the square term, increasing the Seebeck coefficient is an excellent method to enhance the power factor, so a heavier ionic dopant based on (SrLa)TiO_3 can be found to enhance *S* and reduce the lattice thermal conductivity, thus further enhancing the thermoelectric properties. Bi_2O_3 is a commonly used sintering aid for electronic functional ceramics [25]. At the late sintering stage, part of Bi^{3+} diffuses into the lattice of matrix materials, resulting in a donor doping effect and improving the electrical properties of materials. Meanwhile, Bi^{3+} has been proven to regulate the electronic structure of $SrTiO_3$ [26], and is expected to enhance the thermoelectric properties of the material due to its large atomic mass. However, there are few experiments and calculation reports on the thermoelectric properties of Bi^{3+}-doped $SrTiO_3$ at present. Therefore, it is necessary to explore the internal mechanism of the influence of Bi^{3+} on the thermoelectric properties of $SrTiO_3$.

In this work, considering oxygen vacancies always appear in the $SrTiO_3$-based thermoelectric materials [27], $Sr_{0.889}La_{0.111}TiO_{2.963}$ was chosen as matrix material, and a model with 3 × 3 × 3 super-large crystal cell containing 27 protocells and 135 atoms was constructed. Based on the same La^{3+} doping concentration, the first-principles plane-wave pseudopotential method based on density functional theory (DFT) was adopted to study the electronic structure and thermoelectric properties of strontium titanate doped with different concentrations of Bi^{3+}. The influence of the Bi^{3+}-doping modification mechanism on thermoelectric properties was explored.

2. Calculation Methods and Cell Models

2.1. Cell Models

$SrTiO_3$ belongs to the cubic crystal system, and its crystal structure belongs to the spatial group *Pm*3*m*(*O*1 h). The cell parameter *a*=*b*=*c*=0.3905 nm [28]. Sr^{2+} occupies the position of the A position of the eight apex angles of the cell, Ti^{4+} is located at the B position of the body center of the cell, the anion O^{2-} is located at the face-center, and the coordination number is 12, 6 and 6, respectively. In this work, a 3 × 3 × 3 supercell containing 27 protocells and 135 atoms was selected as the computational model of the material. The cell models of $(Sr_{0.889-x}La_{0.111}Bi_x)TiO_{2.963}$ with Bi^{3+} doping were constructed, and the Bi^{3+}-doping concentration was 0%, 3.7%, 7.4%, 11.1% and 14.8%, respectively. The cell models correspond to the composition of $Sr_{0.889}La_{0.111}TiO_{2.963}$ (SLT), $Sr_{0.852}La_{0.111}Bi_{0.037}TiO_{2.963}$ (SLTB1), $Sr_{0.815}La_{0.111}Bi_{0.074}TiO_{2.963}$ (SLTB2), $Sr_{0.778}La_{0.111}Bi_{0.111}TiO_{2.963}$(SLTB3), and $Sr_{0.741}La_{0.111}Bi_{0.148}TiO_{2.963}$ (SLTB4). In order to further explore the effect of Bi^{3+} and La^{3+}, the composition of $Sr_{0.815}La_{0.185}TiO_{2.963}$ (SLTL) with the same content of Sr^{2+} as SLTB2 was designed and calculated. The configurations of supercells are shown in Figure 1.

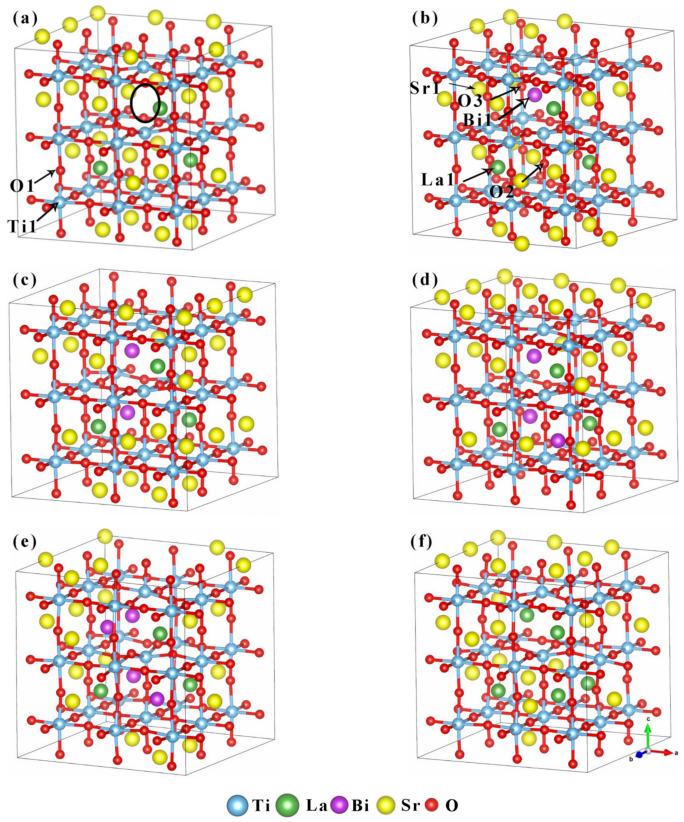


Figure 1. Cell models of $(Sr_{0.889-x}La_{0.111}Bi_x)TiO_{2.963}$. (**a**) $Sr_{0.889}La_{0.111}TiO_{2.963}$; (**b**) $Sr_{0.852}La_{0.111}Bi_{0.037}TiO_{2.963}$; (**c**) $Sr_{0.815}La_{0.111}Bi_{0.074}TiO_{2.963}$; (**d**) $Sr_{0.778}La_{0.111}Bi_{0.111}TiO_{2.963}$; (**e**) $Sr_{0.741}La_{0.111}Bi_{0.148}TiO_{2.963}$; (**f**) $Sr_{0.815}La_{0.185}TiO_{2.963}$ (the position of the black circle is the position where the O^{2-} vacancy is introduced, and the position of the O^{2-} vacancy is the same for each cell).

2.2. Calculation Method

In this work, vasp software [29] was used to optimize the cell model, calculate the electronic structure and mechanical properties of the material, vaspkit [30] was used to process the data obtained, BoltzTrap2 software (TU Wien, Austria) [31] was used to calculate the thermoelectric properties of the material, and experimental data combined with the Slack model was used to calculate the lattice thermal conductivity of the material [32]. The relaxation time of the material was calculated using the deformation potential theory [33]. The ultra-soft pseudoptential method of plane waves based on density functional theory (DFT) was calculated, and the Perdew–Burke–Ernzerhof (PBE) function under generalized gradient approximation (GGA) was used to expand the exchange correlation energy [34]. For the integral calculation of k points in the Brillouin area, the k point of supercells is set as $3 \times 3 \times 3$. The four valence electron configurations of Sr, Ti, O, La and Bi are $4s^24p^65s^2$,$3s^23p^63d^24s^2$,$2s^22p^4$, $5s^25p^65d^16s^2$ and $6s^26p^3$, respectively. In the calculation process, the energy convergence accuracy is 1.0×10^{-6} eV/atom, the maximum atomic displacement is 0.0001 nm, the truncation energy is 400 eV, the convergence standard of internal crystal stress is 0.05 Gpa, and the convergence standard of interatomic interaction is 0.3 eV/nm. Firstly, six kinds of $3 \times 3 \times 3$ supercells were constructed. Secondly, the constructed cells were geometrically optimized. Finally, the physical properties were calculated based on the geometrically optimized cells.

3. Results and Discussion

3.1. Lattice Structure and Electronic Structure

Table 1 lists the cell parameters of the relaxed $(Sr_{0.889-x}La_{0.111}Bi_x)TiO_{2.963}$ supercell. It can be seen that the calculated $Sr_{0.889}La_{0.111}TiO_3$ cell parameter of 0.3906 nm is −0.0512%

smaller than the experimental data of 0.3908 nm [35], which indicates that the established crystal structure model is reasonable.

Table 1. Cell parameters of $(Sr_{0.889-x}La_{0.111}Bi_x)TiO_{2.963}$.

Crystals	a (Å)	b (Å)	c (Å)	c/a	Volume ($Å^3$)	Ti1-O1 Length(Å)	La1-O2 Length(Å)	Bi1-O3 Length(Å)	Sr1-O3 Length(Å)
SLT	3.909	3.909	3.905	0.9990	59.695	1.972	2.915	\	2.738
SLTB1	3.910	3.910	3.908	0.9995	59.762	1.970	2.884	3.223	2.699
SLTB2	3.912	3.912	3.910	0.9995	59.839	1.974	2.843	3.464	2.732
SLTB3	3.914	3.914	3.912	0.9995	59.957	1.978	2.850	3.484	2.733
SLTB4	3.920	3.920	3.914	0.9985	59.565	1.997	2.958	3.490	2.755
SLTL	3.912	3.912	3.906	0.9985	59.750	1.973	2.939	\	2.753

It can be seen from the table that after doping Bi^{3+}, the cell structure of $(Sr_{0.889-x}La_{0.111}Bi_x)TiO_{2.963}$ does not change significantly, and it still maintains the cubic system. The cell parameters in the *a* and *b* direction are equal, but they decrease slightly in the *c* direction. *c*/*a* represents lattice distortion, and the more *c*/*a* deviates from 1.000, the greater the lattice distortion degree. It can be clearly seen from Figure 1 that the Ti–O octahedron has an obvious distortion, and Ti^{4+} ions are all far away from the center of the octahedron. In the *c* direction, the atoms shift to the inside of the cell, resulting in a slight contraction of the cell. In the *a* and *b* directions, the atoms shift to the outside, resulting in a slight expansion of the cell. The lattice distortion degree of SLTB1-3 is similar, while the lattice distortion degree of SLT, SLTB4 and SLTL is larger.

With the increase of Bi^{3+} concentration, the cell parameters increased, which is consistent with the results of another experiment [36]. The reason for the increase of cell parameters after the introduction of Bi^{3+} may be due to the mismatch and electronegativity difference between Bi^{3+}, La^{3+} and Sr^{2+}, which leads to the growth of Ti–O and Bi–O bonds. The electronegativity of Bi^{3+} is 2.02, the electronegativity of La^{3+} is 1.1, the electronegativity of Sr^{2+} is 0.95, and the electronegativity of O^{2-} is 3.44. According to Pauling's rule, the larger the electronegativity difference, the stronger the electron-attracting ability of ions, the smaller the distance between ions, and the smaller the bond length. The difference between the electronegativity of Bi^{3+} and that of O^{2-} is less than 1.7, indicating that Bi^{3+} and O^{2-} are mainly covalent bonds, and the bond length is large. The positions of Ti1 and O1 are marked in Figure 1a, and the positions of Bi1, La1, Sr1, O2, and O3 are marked in Figure 1b. Table 1 lists the bond lengths of Ti1–O1, La1–O2, Bi1–O3 and Sr1–O3 at the same position in the cell models of the six kinds of supercells. It can be seen that the Bi–O bond length is larger than the La–O bond length and Sr–O bond. At the same time, when Bi^{3+} doping concentration increases, the Ti1–O1 bond length and Bi1–O3 bond length increase, resulting in cell distortion and slight expansion.

After geometric optimization, the non-self-consistent calculation of the band structure was performed, and the band structure of $(Sr_{0.889-x}La_{0.111}Bi_x)TiO_{2.963}$ was obtained, as shown in Figure 2. The calculation of the band structure of $SrTiO_3$ brillouin zone high-symmetry point selection was as follows: $\Gamma \rightarrow X \rightarrow M \rightarrow \Gamma \rightarrow R \rightarrow X$ (Γ, X, M, R, X, are the brillouin zone high-symmetry points). It can be found that the Fermi level of $(Sr_{0.889-x}La_{0.111}Bi_x)TiO_{2.963}$ is in the top of the valence band; the band at the top of valence band is point R, and the bottom of the conduction band is in point Γ, which is consistent with Benrekia [37]. The experimental value of the band gap of intrinsic $SrTiO_3$ is measured as 3.25 eV [38], and the calculated band gap is in the range of 2.907–2.305 eV; due to the PBE function, this will significantly underestimate the band gap [37]. Although there is a certain difference between the calculated value and the experimental value, the selected parameters in the calculation are consistent, the obtained law of band structure change is reliable and this will not affect the theoretical analysis of the electronic structure.

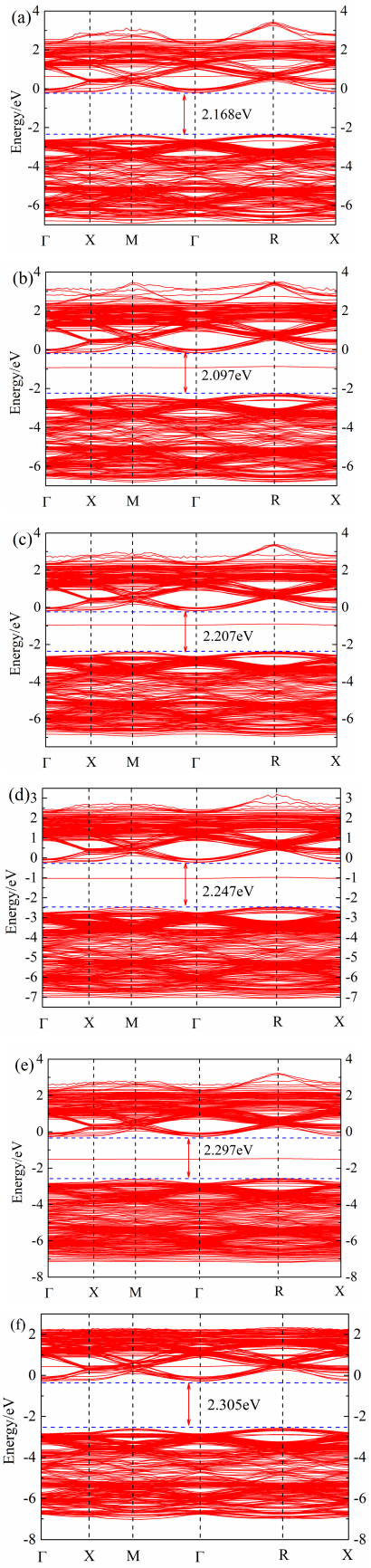


Figure 2. Band structure of $(Sr_{0.889-x}La_{0.111}Bi_x)TiO_{2.963}$. (**a**) $Sr_{0.889}La_{0.111}TiO_{2.963}$; (**b**) $Sr_{0.852}La_{0.111}Bi_{0.037}TiO_{2.963}$; (**c**) $Sr_{0.815}La_{0.111}Bi_{0.074}TiO_{2.963}$; (**d**) $Sr_{0.778}La_{0.111}Bi_{0.111}TiO_{2.963}$; (**e**) $Sr_{0.741}La_{0.111}Bi_{0.148}TiO_{2.963}$; (**f**) $Sr_{0.815}La_{0.185}TiO_{2.963}$.

By comparing Figure 2a–e, it can be seen that with the increase of Bi^{3+} concentration, the band gap of $((Sr_{0.889-x}La_{0.111}Bi_x)TiO_{2.963}$ first decreases and then increases. The minimum band gap of SLTB1 is 2.097 eV, and the maximum band gap of SLTB4 is 2.297 eV. With the increase of the incorporation concentration of Bi^{3+} ions, the deeper the Fermi level enters the conduction band, indicating that Bi^{3+} ions emit more electrons than Sr^{2+} ions, which increases the carrier concentration of the system and generates a degenerate system. Bi^{3+} doping changes the conductivity of strontium titanate, and the Fermi level is greater than the minimum conduction band, indicating that the strontium titanate material system has exhibited metallic properties at this time [20].

The specific defect chemical reaction can be given by Formula (1):

$$3La + xBi + 27SrTiO_3 = 3La_{Sr}^{\cdot} + xBi_{Sr}^{\cdot} + V_O^{2\cdot} + 27Ti_{Ti}^{x} + 80O_O^{x} + (x+5)e\prime \quad (1)$$

By comparing Figure 2a,f and Figure 2b–e, it can be found that impurity levels appear after Bi^{3+} doping, indicating that Bi^{3+} doping causes certain changes in the material energy band structure, which is consistent with the calculation of Zhang26. Bi^{3+} doping introduces an impurity level at the −2 eV~0 eV position, which promotes the electron transition. Electrons can jump from the valence band to the impurity level first, and then jump into the conduction band, which will increase the electron mobility and conductivity of the material.

In order to further study the influence of Bi^{3+} doping on the electronic structure of $SrTiO_3$, the total state density (DOS) and split-wave state density (PDOS) of $(Sr_{0.889-x}La_{0.111}Bi_x)TiO_{2.963}$ were calculated, as shown in Figure 3. As can be seen from Figure 3b, the top of the valence band of doped strontium titanate is mainly composed of O-2p orbitals, and the bottom of the conduction band is mainly composed of Ti-3d orbitals, indicating that the co-vertex-connected titano-oxygen octahedron determines the electronic structure of strontium titanate, the energy level of Sr orbital does not contribute to the valence band and conduction band, and the 6p of Bi^{3+} and 5d of La^{3+} participate in forming the conduction band. However, its split-wave state density is small. At the same time, it is obvious that the 6p orbital of Bi^{3+} introduces a small DOS peak in the center of the valence and conduction bands, which corresponds to the impurity level in the previous band structure. It is foreseeable that the inclusion of Bi^{3+} will have an impact on the electrical transport performance of the material. The Seebeck coefficient is related to the asymmetry of DOS relative to the Fermi level and the steepness of state density. The larger the asymmetry, the steeper the state density peak, and the larger the Seebeck coefficient. By comparing Figures 3a and 3b–e, the change of the value of second peak around the conduction band position of the total state density is about 2 eV, and the DOS of $(Sr_{0.889-x}La_{0.111}Bi_x)TiO_{2.963}$ increases asymmetrically relative to the Fermi level. The introduction of Bi^{3+} may increase the absolute Seebeck coefficient of the material. Under the condition of the same concentration of Sr^{2+} replace, the value of the second peak of SLTB2 is less than that of SLTL, which shows that the contribution to the DOS in the bottom of the conduction band of Bi^{3+} is less than La^{3+} with the same concentration. As shown in Figure 3a–e, with the increase of Bi^{3+} ion incorporation concentration, the deeper the Fermi level enters the conduction band, the greater the value of DOS at Fermi level and the steeper the peak. The addition of Bi^{3+} ions will increase the absolute value of the Seebeck coefficient.

3.2. Thermoelectric Properties

The Seebeck coefficient of $(Sr_{0.889-x}La_{0.111}Bi_x)TiO_{2.963}$ changes with the chemical potential at different temperatures, as shown in Figure 4. When the chemical potential $\mu > 0$, it indicates that the material is *n*-type doped; when the chemical potential $\mu < 0$, it indicates that the material system is *p*-type doped. The larger the chemical potential μ, the deeper the Fermi level moves up into the conduction band; the smaller the chemical potential μ, the deeper the Fermi level moves down into the valence band [38]. It can be seen from Figure 4a,f that the *S*-curve of $(Sr_{1-x}La_x)TiO_{2.963}$ is similar, and its absolute value is very large near $\mu = 0$, and the absolute value increases rapidly, and then increases when the chemical potential slowly decreases. When $\mu < -0.1$ Ry and $\mu > 0.1$ Ry, *S* tends to zero

and is almost independent of temperature, which is mainly due to the gradual decrease of carrier concentration [24,39]. Comparing Figure 4a with Figure 4b–e, it can be seen that when Bi^{3+} is doped, within the range of chemical potential 0.05 Ry < μ < 0.1 Ry, the second peak appears in the Seebeck coefficient, which increases with the increase of Bi^{3+}-doping concentration. The possible reason for this is that the chemical potential range of 0.05 Ry < μ < 0.1 Ry corresponds to the impurity level between the top of the valence band and the bottom of the conduction band in the energy band structure. When the doping concentration of Bi^{3+} increases, the energy level of the impurity increases, and the presence of impurity levels has a significant impact on the Seebeck coefficient of the material.

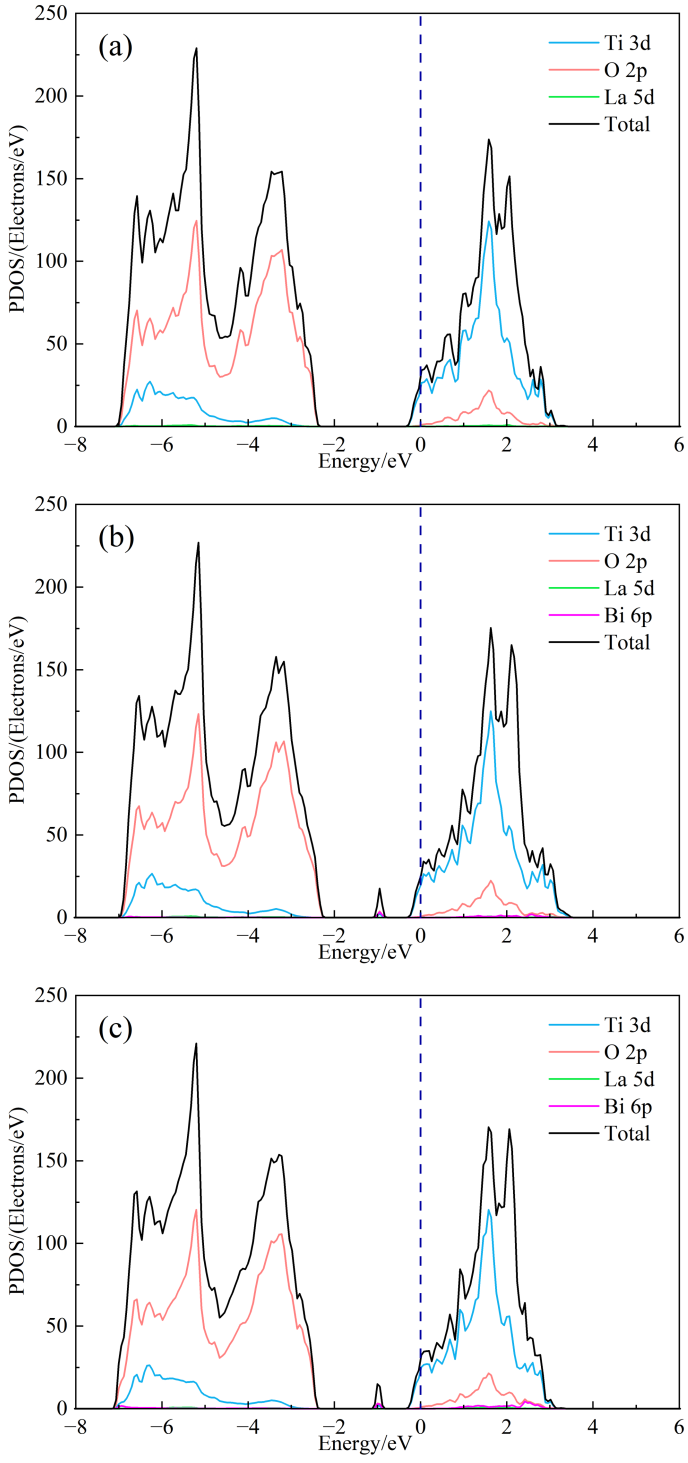


Figure 3. *Cont.*

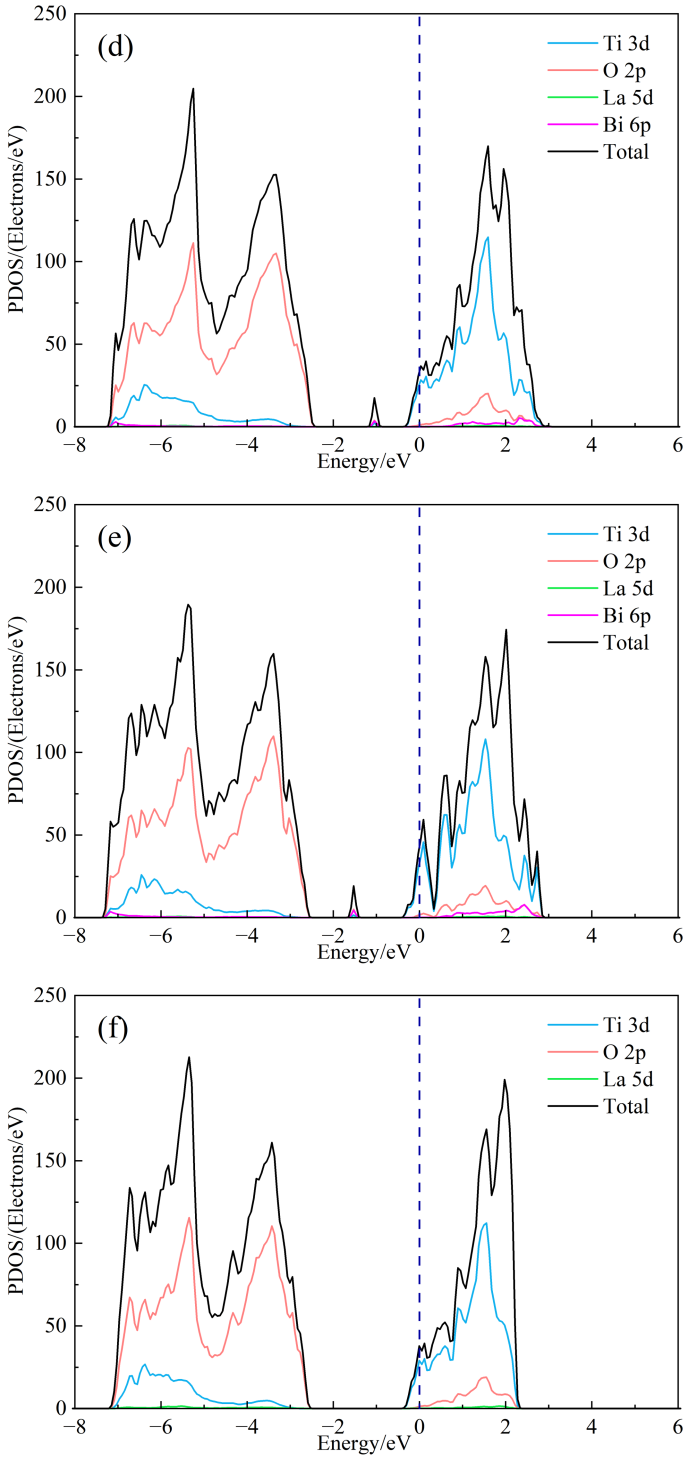


Figure 3. The DOS of $(Sr_{0.889-x}La_{0.111}Bi_x)TiO_{2.963}$. (**a**) $Sr_{0.889}La_{0.111}TiO_{2.963}$; (**b**) $Sr_{0.852}La_{0.111}Bi_{0.037}TiO_{2.963}$; (**c**) $Sr_{0.815}La_{0.111}Bi_{0.074}TiO_{2.963}$; (**d**) $Sr_{0.778}La_{0.111}Bi_{0.111}TiO_{2.963}$; (**e**) $Sr_{0.741}La_{0.111}Bi_{0.148}TiO_{2.963}$; (**f**) $Sr_{0.815}La_{0.185}TiO_{2.963}$.

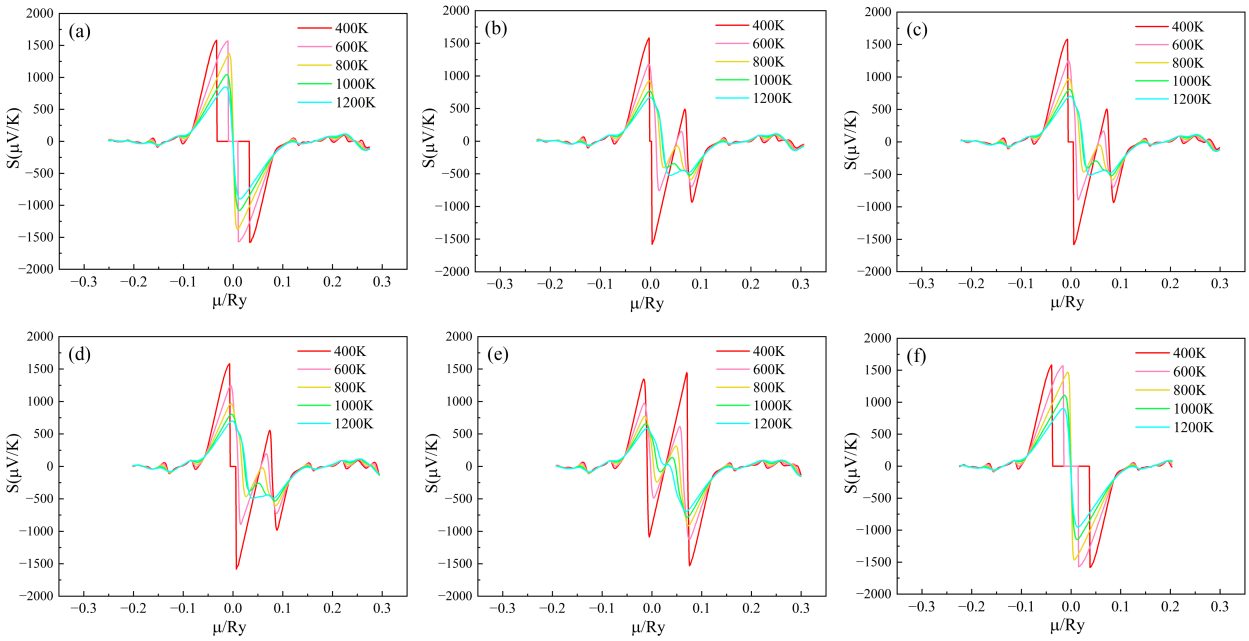


Figure 4. Chemical potential dependent of S of $(Sr_{0.889-x}La_{0.111}Bi_x)TiO_{2.963}$. (**a**) $Sr_{0.889}La_{0.111}TiO_{2.963}$; (**b**) $Sr_{0.852}La_{0.111}Bi_{0.037}TiO_{2.963}$; (**c**) $Sr_{0.815}La_{0.111}Bi_{0.074}TiO_{2.963}$; (**d**) $Sr_{0.778}La_{0.111}Bi_{0.111}TiO_{2.963}$; (**e**) $Sr_{0.741}La_{0.111}Bi_{0.148}TiO_{2.963}$; (**f**) $Sr_{0.815}La_{0.185}TiO_{2.963}$.

Figure 5 shows the conductivity/relaxation time(σ/τ) of $(Sr_{0.889-x}La_{0.111}Bi_x)TiO_{2.963}$ as a function of chemical potential. In the vicinity of $\mu = 0$, σ/τ is almost 0, but mainly exhibits conductivity below -0.1 Ry and above 0.1 Ry. The σ/τ curves of $(Sr_{0.889-x}La_{0.111}Bi_x)TiO_{2.963}$ have similar trends. The conductivity of n-type doping is greater than that of p-type doping, indicating that SLTB materials are n-type semiconductors. When $0 < \mu < 0.1$ Ry, the conductivity increases with the chemical potential. When μ is around 0.2 Ry, the conductivity begins to decrease with the increase of chemical potential. The higher the temperature, the smaller the σ/τ of the material system, which is due to the severe carrier scattering at high temperature and the decrease of carrier mobility. For the $(Sr_{0.889-x}La_{0.111}Bi_x)TiO_{2.963}$, when the Bi^{3+}-doping concentration is 0%, 3.7%, 7.4%, 11.1%, 14.8%, the maximum σ/τ of the material system is $1.802 \times 10^{20}/(\Omega{\cdot}ms)$, $1.985 \times 10^{20}/(\Omega{\cdot}ms)$, $1.680 \times 10^{20}/(\Omega{\cdot}ms)$, $1.452 \times 10^{20}/(\Omega{\cdot}ms)$, and $1.165 \times 10^{20}/(\Omega{\cdot}ms)$ at 400 K, respectively. For the SLTL, the maximum σ/τ of the material system is $1.597 \times 10^{20}/(\Omega{\cdot}ms)$ at 400 K. After the introduction of Bi^{3+} doping, the σ/τ of the material system first increased and then decreased, indicating that an appropriate Bi^{3+}-doping concentration (3.7–7.4%) is conducive to the improvement of electrical conductivity, while an excessive Bi^{3+}-doping concentration (11.1–14.8%) will severely scatter carriers and deteriorate the conductivity.

The trend of electronic thermal conductivity/relaxation time of $(Sr_{0.889-x}La_{0.111}Bi_x)TiO_{2.963}$ as a function of chemical potential at different temperatures is shown in Figure 6. For $(Sr_{0.889-x}La_{0.111}Bi_x)TiO_{2.963}$, when the Bi^{3+}-doping concentration is 0%, 3.7%, 7.4%, 11.1%, and 14.8%, respectively, the material system κ_e/τ maximum is 3.358×10^{15} W/(mKs), 3.634×10^{15} W/(mKs), 3.191×10^{15} W/(mKs), 2.929×10^{15} W/(mKs) and 2.420×10^{15} W/(mKs) at 1200 K, respectively. For the SLTL, the maximum κ_e/τ is 3.006×10^{15} W/(mKs) at 1200 K. κ_e/τ increases, and the trend of κ_e/τ is similar to σ/τ. κ_e/τ mainly has two peaks in the range of $\mu < -0.1$ Ry and $\mu > 0.1$ Ry.

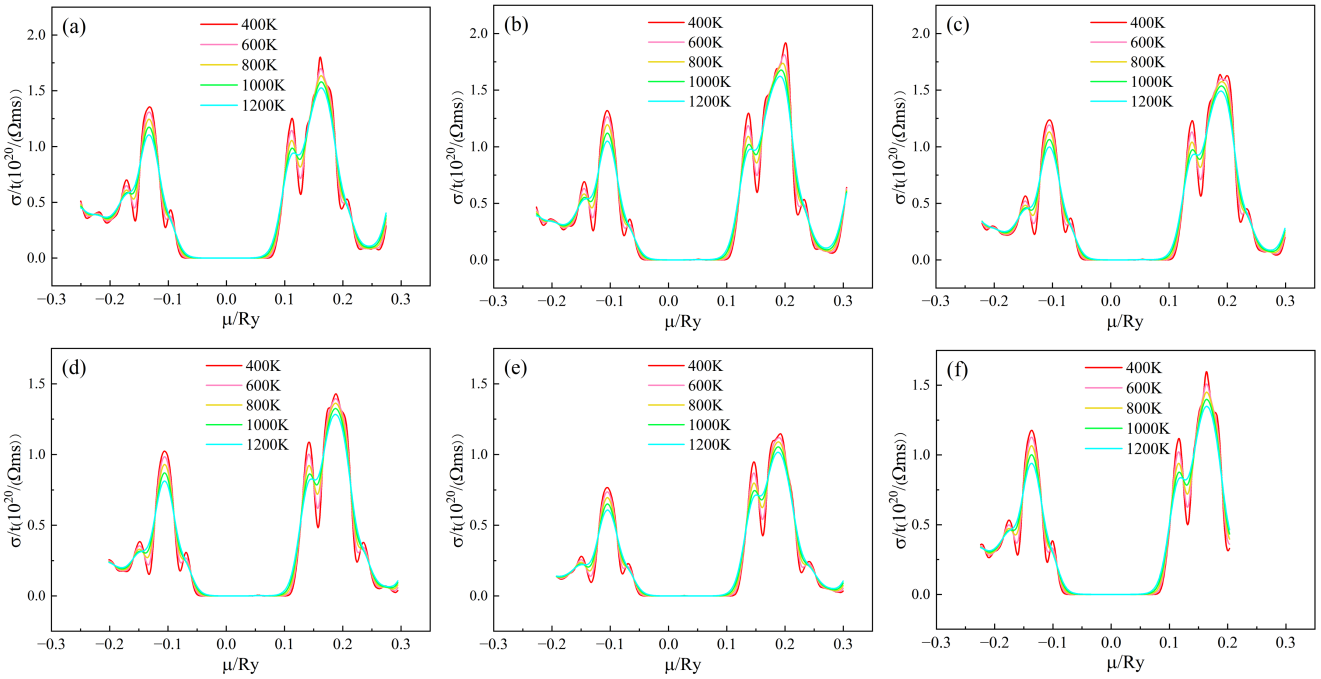


Figure 5. Chemical potential dependent of σ/τ of $(Sr_{0.889-x}La_{0.111}Bi_x)TiO_{2.963}$. (**a**) $Sr_{0.889}La_{0.111}TiO_{2.963}$; (**b**) $Sr_{0.852}La_{0.111}Bi_{0.037}TiO_{2.963}$; (**c**) $Sr_{0.815}La_{0.111}Bi_{0.074}TiO_{2.963}$; (**d**) $Sr_{0.778}La_{0.111}Bi_{0.111}TiO_{2.963}$; (**e**) $Sr_{0.741}La_{0.111}Bi_{0.148}TiO_{2.963}$; (**f**) $Sr_{0.815}La_{0.185}TiO_{2.963}$.

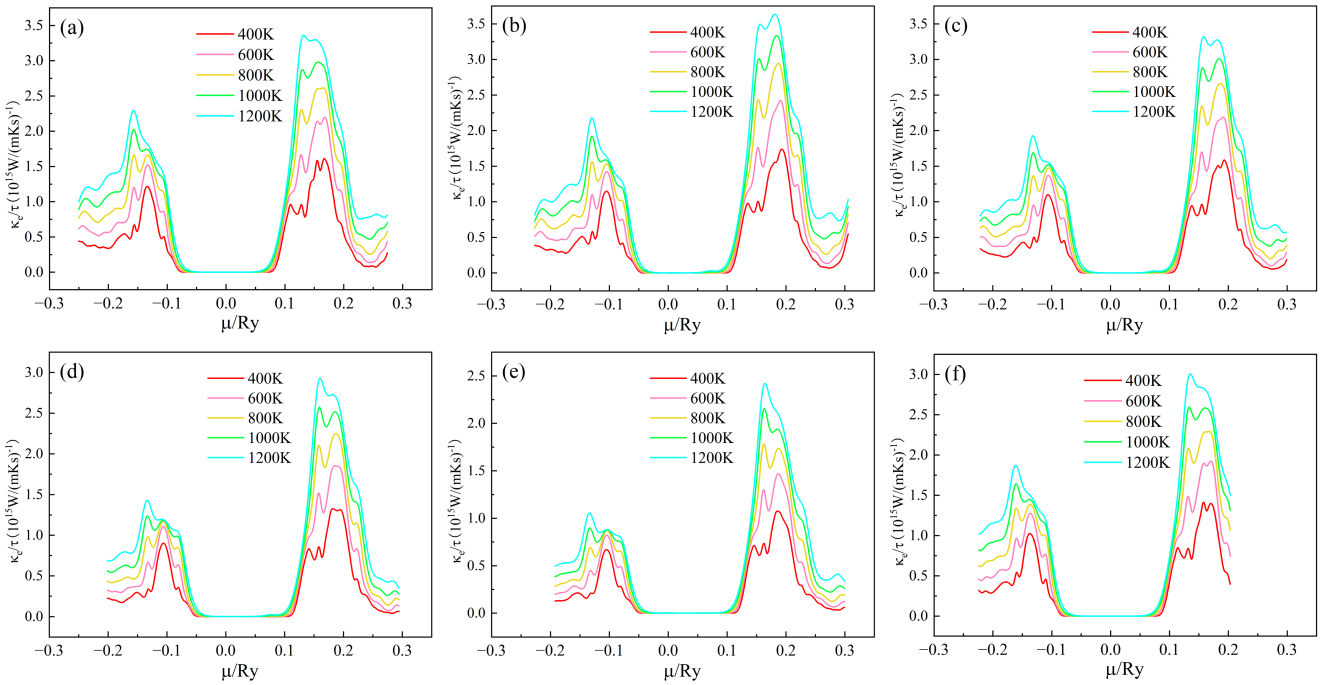


Figure 6. Chemical potential dependent of κ_e/τ of $(Sr_{0.889-x}La_{0.111}Bi_x)TiO_{2.963}$. (**a**) $Sr_{0.889}La_{0.111}TiO_{2.963}$; (**b**) $Sr_{0.852}La_{0.111}Bi_{0.037}TiO_{2.963}$; (**c**) $Sr_{0.815}La_{0.111}Bi_{0.074}TiO_{2.963}$; (**d**) $Sr_{0.778}La_{0.111}Bi_{0.111}TiO_{2.963}$; (**e**) $Sr_{0.741}La_{0.111}Bi_{0.148}TiO_{2.963}$; (**f**) $Sr_{0.815}La_{0.185}TiO_{2.963}$.

The power factor/relaxation time of the $(Sr_{0.889-x}La_{0.111}Bi_x)TiO_{2.963}$ varies with the chemical potential as shown in Figure 7. The value of $S^2\sigma/\tau$ of *n*-type doped material is greater than that of the *p*-type doped material, indicating that the material is more suitable for *n*-type doping and is an *n*-type semiconductor, which is consistent with the previous

analysis of σ/τ. For the SLTB, the maximum $S^2\sigma/\tau$ values of the material are 8.175 × 10^{11}, 8.551 × 10^{11}, 8.282 × 10^{11}, 7.518 × 10^{11}, 6.546 × 10^{11} W/(mK^{2}s) at 1200 K. For SLTL, the maximum $S^2\sigma/\tau$ of the material is 7.402 × 10^{11} W/(mK^{2}s) at 1200K. The values of $(Sr_{0.889-x}La_{0.111}Bi_x)TiO_{2.963}$ reached the highest values at 0.11007 Ry, 0.11293 Ry, 0.11685 Ry, 0.12111 Ry, 0.08539 Ry, and 0.08929 Ry, respectively. Therefore, the later calculated thermoelectric properties are based on these chemical potentials to obtain better thermoelectric properties [24]. The variation diagram of $S^2\sigma/\tau$ values of $(Sr_{0.889-x}La_{0.111}Bi_x)TiO_{2.963}$ with the chemical potential at 1200K is shown in Figure S1 (See Supplementary Materials). After the introduction of Bi^{3+} doping, the maximum value of $S^2\sigma/\tau$ of the material increases first and then decreases. When the Bi^{3+} concentration is higher, the deterioration of $S^2\sigma/\tau$ is more obvious. At the same time, it can be seen that the chemical potential value at which SLTB achieves the maximum $S^2\sigma/\tau$ is significantly greater than that of SLTL. The possible reason for this is that with the increase of Bi^{3+} concentration, the deeper the Fermi level enters the conduction band. Bi^{3+} affects the band structure of the material so that the chemical potential at which the maximum value is obtained increases.

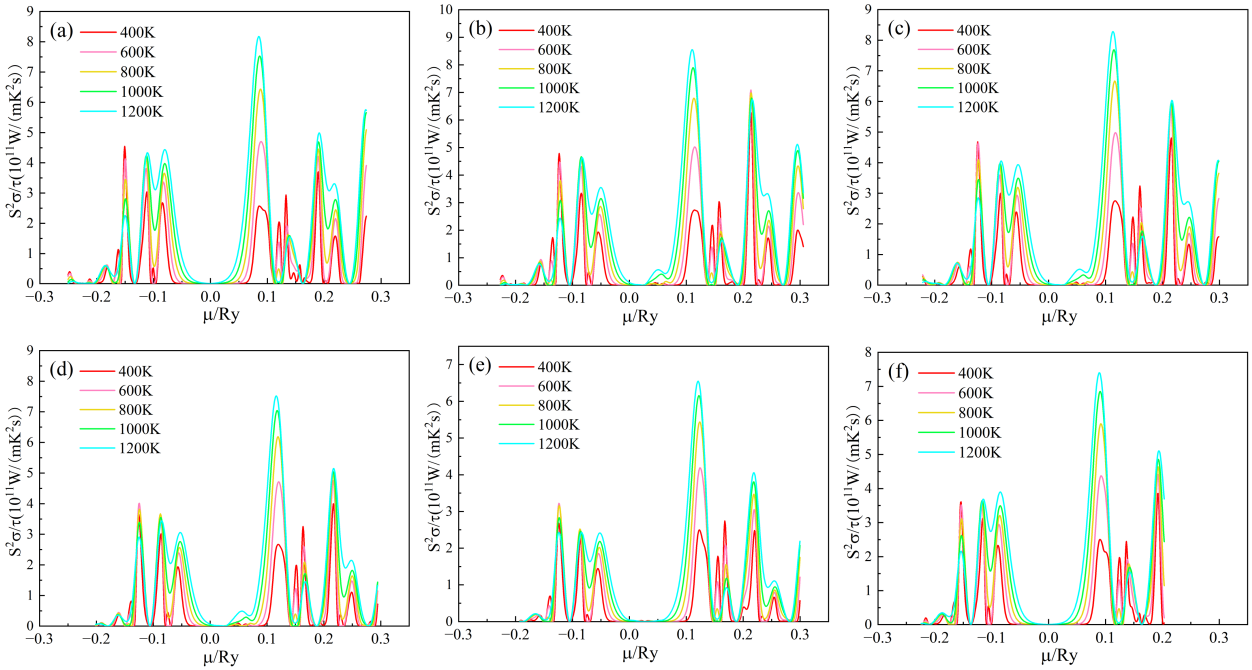


Figure 7. Chemical potential dependent of $S^2\sigma/\tau$ of $(Sr_{0.889-x}La_{0.111}Bi_x)TiO_{2.963}$. (**a**) $Sr_{0.889}La_{0.111}TiO_{2.963}$; (**b**) $Sr_{0.852}La_{0.111}Bi_{0.037}TiO_{2.963}$; (**c**) $Sr_{0.815}La_{0.111}Bi_{0.074}TiO_{2.963}$; (**d**) $Sr_{0.778}La_{0.111}Bi_{0.111}TiO_{2.963}$; € $Sr_{0.741}La_{0.111}Bi_{0.148}TiO_{2.963}$; (**f**) $Sr_{0.815}La_{0.185}TiO_{2.963}$.

The effective mass of carriers is calculated by the parabolic model, which is mainly related to the quadratic term of the lowest conduction band [40]. The calculated carrier effective mass of $(Sr_{0.889-x}La_{0.111}Bi_x)TiO_{2.963}$ is shown in Table 2. With the increase of Bi^{3+} concentration, the electronic effective mass of strontium titanate material system increases slightly, from 2.422 to 2.722 m_e. At the same time, electron effective mass of $(Sr_{0.889-x}La_{0.111}Bi_x)TiO_{2.963}$ is greater than that of SLT and SLTL, which is due to the larger mass of Bi^{3+}.

Table 2. m^*/m_e, μ, n of $(Sr_{0.889-x}La_{0.111}Bi_x)TiO_{2.963}$ at 300 K.

Crystals	m^*/m_e	μ(cm^2 V^{-1}s^{-1})	n($\times 10^{21}$ cm^{-3})
SLT	2.395	8.902	2.598
SLTB1	2.422	8.560	2.183
SLTB2	2.477	8.937	2.362
SLTB3	2.507	6.342	2.465
SLTB4	2.720	5.202	2.674
SLTL	2.451	8.786	2.904

There is a relaxation time τ term in the electrical transport performance, and this paper adopts the DFT to deal with the electronic relaxation time [33]. According to the deformation potential theory and the rigid energy band model, the relaxation time does not change with the doping concentration, and the electronic relaxation time of the three-dimensional material is shown as:

$$\tau = \frac{2\sqrt{2\pi}\hbar^4 C_{3D}}{3(k_B T)^{3/2} E^2 m^{*3/2}} = \frac{\mu m^*}{e} \quad (2)$$

where C_{3D} is the elastic constant, E is the deformation potential energy, m^* is the electronic effective mass, k_B is the Boltzmann constant, $\hbar$ as the Planck constant divided by 2 π, T is temperature, μ is the carrier mobility, and E is the unit charge.

By applying pressure to each unit cell to cause deformations of −1.5%, −1.0%, −0.5%, 0.0%, 0.5%, 1.0%, and 1.5%, the elastic constant C_{3D} is calculated according to the energy–stress relationship. The deformation potential energy E is calculated according to the energy change of the conduction band energy level, and the electron effective mass m^* is fitted according to the curve of the conduction band energy band. Finally, we substitute the parameters into the formula to obtain the relaxation time τ of each unit cell separately, and obtain the relationship between the relaxation time and temperature. As shown in Figure S2, when the temperature increases, the relaxation time decreases from 5.23–8.17 fs to 1.01–1.57 fs. Ohta [10] did a similar experiment and Kinaci [13] reported that the relaxation time of La^{3+}-doped strontium titanate decreases from 8 fs to 1.5 fs, which is consistent with the calculated results in this work. It shows the rationality of this method to calculate the relaxation time.

It can be found from the figure that the relaxation times of the four unit cells of SLTB1, SLTB2, SLTB3, SLTB4 are similar. The relaxation times of SLT and SLTL are slightly smaller. This is mainly due to the fact that the excessive Bi^{3+} concentration reduces the deformation potential energy, E. The calculation of deformation potential theory is based on the scattering process between phonons and electrons, without considering optical phonon scattering and possible impurity scattering, which may lead to overestimation of relaxation time, electrical conductivity, and ZT at medium and low temperatures [41]. However, the changing trend of the conductivity and ZT of Bi^{3+} and La^{3+} doping in the high temperature section revealed in this study will not be affected.

Carrier mobility can be calculated according to the relaxation time, as shown in Formula (3). Carrier concentration can be calculated by carrier mobility and conductivity:

$$n = \frac{\sigma}{e\mu} \quad (3)$$

where σ is conductivity, μ is carrier mobility. The calculated carrier mobility and carrier concentration of $(Sr_{0.889-x}La_{0.111}Bi_x)TiO_{2.963}$ are shown in Table 2. For $(Sr_{0.889-x}La_{0.111}Bi_x)TiO_{2.963}$, with the increase of Bi^{3+} concentration, the carrier migration first increases and then decreases. When the doping concentration is 7.4%, the maximum carrier mobility is 8.937 $cm^2V^{-1}s^{-1}$. The high carrier mobility of SLTB2 is due to the impurity level introduced by Bi^{3+} into the band structure, which acts as the carrier migration path. When the doping concentration of Bi^{3+} is greater than 11.1%, the excessive mass of Bi^{3+} greatly

scatters the carrier, thus reducing the carrier mobility. The carrier mobility of SLTB1, SLTB2, SLTB3 and SLTB4 is similar at 8.5–9 $cm^2V^{-1}s^{-1}$.

What is more, with the increase of Bi^{3+} concentration, the carrier concentration increases from 2.183 × 10^{21} cm^{-3} to 2.674 × 10^{21} cm^{-3}. As can be seen from the defect chemical reaction equation, Bi^{3+} is a +3 valence state, and when it replaces Sr^{2+}, it will introduce excessive electrons into the system, thus increasing the carrier concentration. Meanwhile, under the condition of the same concentration of Sr^{2+}, the carrier concentration of SLTB2 (2.183 × 10^{21} cm^{-3}) is lower than that of SLTL (2.905 × 10^{21} cm^{-3}). This may be due to the fact that the contribution of Bi^{3+} to DOS at the bottom of the conduction band is smaller than that of La^{3+} at the same concentration. At the same time, the carrier concentration basically does not change with temperature and is greater than 10^{10} cm^{-3}, indicating that the material is a degenerate semiconductor [42].

After the term of relaxation time is substituted, the Seebeck coefficient, electrical conductivity, power factor and electron thermal conductivity of $(Sr_{0.889-x}La_{0.111}Bi_x)TiO_{2.963}$ change with temperature are shown in Figure 8. The absolute value of Seebeck coefficient increases with the increase of temperature, from 91.428 μV/K–101.255 μV/K at 400 K to 129.225 μV/K–144.570 μV/K at 1200 K, indicating that the Bi^{3+}-doped $SrTiO_3$ material is an *n*-type degenerate semiconductor. By comparing SLTB, SLT, and SLTL, the absolute value of the Seebeck coefficient of the material with Bi^{3+} showed a relatively large value, which is consistent with the previous analysis of the band structure and state density. For $(Sr_{0.889-x}La_{0.111}Bi_x)TiO_{2.963}$, the absolute value of the Seebeck coefficient ranges from 91.428 μV/K to 144.570 μV/K, which is slightly smaller than the experimental data of 95 μV/K to 175 μV/K25. With the increase in Bi^{3+} concentration, although the effective electron mass of the material system increases, the Seebeck coefficient of the material decreases.

By comparing SLTB SLT and SLTL, the effective mass of electrons, carrier mobility and migration ability are increased after the introduction of Bi^{3+}, but the carrier concentration is reduced. Due to the conductivity equation $\sigma = ne\mu$, finally, the conductivity of $(Sr_{0.889-x}La_{0.111}Bi_x)TiO_{2.963}$ was reduced [39]. The electrical conductivity of SLT and SLTL at 1200 K are 640.312/(Ω·m) and 642.797/(Ω·m), respectively, which is greater than the experimental data of 250/(Ω·m)–460/(Ω·m) [11,12,18]. For SLTB, with the increase of Bi^{3+} concentration, the carrier concentration of the material increases, the carrier mobility decreases, and the conductivity of the material first increases and then decreases. The material with a Bi^{3+}-doping concentration of 7.4% obtained the maximum conductivity value (633.015/(Ω·m)). However, when the Bi^{3+}concentration continues to increase, the carrier mobility decreases significantly. When Bi^{3+} concentration is 14.8%, the value of electrical conductivity moves down to 383.179/(Ω·m).

The reason why the conductivity of the material system is relatively high at room temperature is that the calculation considers the full excitation of electrons instead of the scattering of optical phonons and possible impurity. In practice, electrons can only gradually achieve thermal excitation when the temperature rises. So, the conductivity of the material at room temperature is overestimated [41].

By comparing SLTB and SLT, the power factor of SLTB1 and SLTB2 is higher than that of SLT. However, when the Bi^{3+} concentration is 11.1% and 14.8%, the power factor of $(Sr_{0.889-x}La_{0.111}Bi_x)TiO_{2.963}$ decreases sharply, indicating that an appropriate Bi^{3+} concentration (3.7–7.4%) is beneficial to optimize the power factor of the material. The power factors of SLTB were 1.199 mW/(mK^2), 1.205 mW/(mK^2), 0.762 mW/(mK^2), and 0.639 mW/(mK^2) at 1200 K, which is consistent with the experimental data of 0.5 mW/(mK^2)–0.9 mW/(mK^2) [25,36].

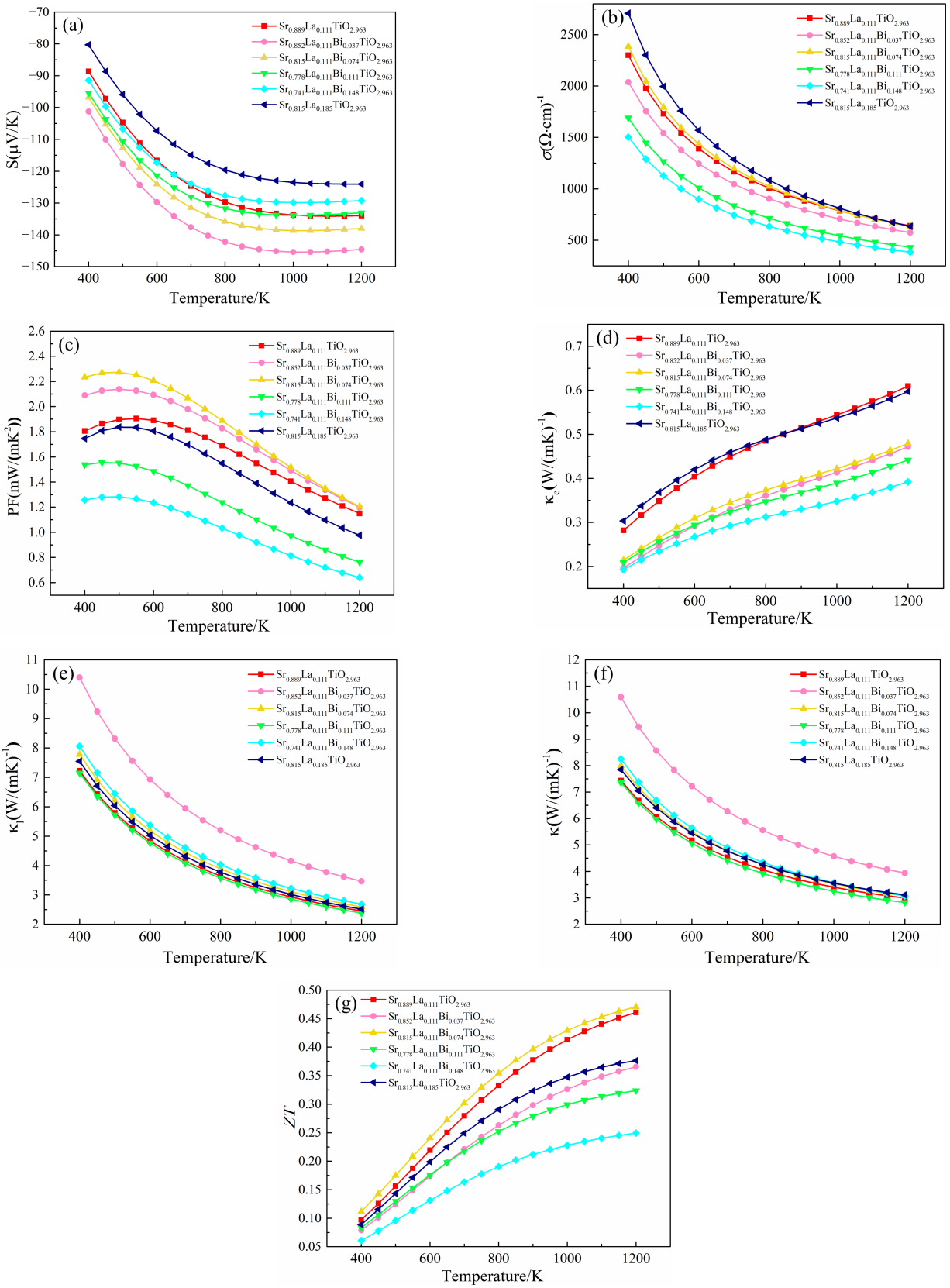


Figure 8. Thermoelectric properties of $(Sr_{0.889-x}La_{0.111}Bi_x)TiO_{2.963}$ vary with temperature. (**a**) Seebeck coefficient; (**b**) conductivity; (**c**) power factor; (**d**) electronic thermal conductivity; (**e**) lattice thermal conductivity; (**f**) thermal conductivity; (**g**) *ZT*.

Thermal conductivity refers to the heat transferred by phonon transport in a temperature gradient. The main factors affecting it include average relative atomic mass, Young's modulus, density, defects in the crystal and porosity. For the most perfect electrical-insulating materials, the heat transfer is mainly performed by phonon–phonon scattering. Combined with sound velocity and elastic properties, the lattice thermal conductivity of materials can be calculated. Slack derived the quantitative expression of intrinsic lattice thermal conductivity [32]:

$$k_{\text{Slack}} = A\frac{M\Theta_{\text{D}}{}^3\delta}{\gamma^2 n^{2/3}T} \quad (4)$$

where A is constant, A = 3.04 × 10^7 W·mol/kg/$m^{2/}K^3$, M is the average atomic mass, n is the number of atoms in primitive cells, δ is average atomic volume, γ is Gruneisen parameters, including gamma sigma calculated by Poisson's ratio 24, and Θ_{D} is the Debye temperature. σ and Θ_{D} are calculated by the mechanical properties with first principles; the detailed data are shown in Table S1.

Due to the scattering of acoustic phonons with the increase of temperature, the relationship between thermal conductivity and temperature in the experiment is often expressed as $\kappa = A/T + L\sigma T$, where A/T and $L\sigma T$ are respectively the thermal conductivity of lattices and the thermal conductivity of electrons [43]. The electronic thermal conductivity has been substituted into the relaxation time term, and the calculated relation of electron thermal conductivity with temperature is shown in Figure 8d. The electron thermal conductivity of SLTB is smaller than that of SLT and SLTL. At present, a lot of research on the lattice thermal conductivity of La^{3+}-doped $SrTiO_3$ materials in the experiment have been reported [4–12]. The lattice thermal conductivity of $Sr_{0.9}La_{0.1}TiO_3$ at 1073K is within the trend range of 2.0–2.6 W/m·K, and the relationship between the lattice thermal conductivity of $Sr_{0.9}La_{0.1}TiO_3$ and temperature is as follows: $\kappa_l = 2860.0/T$. The detailed fitting process is seen in the Supplementary Materials. Finally, the variation of lattice thermal conductivity with temperature calculated by combining experimental data with Slack model is shown in Figure 8e.

The lattice thermal conductivity of SLT, SLTB1, SLTB2, SLTB3, SLTB4 and SLTL at 1200 K are 2.454 W/m·K, 3.465 W/m·K, 2.594 W/m·K, 2.383 W/m·K, 2.686 W/m·K and 2.516 W/m·K, respectively. It can be seen that the lattice thermal conductivities of SLT, SLTB2, SLTB3, SLTB4 and SLTL are similar, except for SLTB1 with a larger lattice thermal conductivity. When the temperature is 1200 K, the lowest lattice thermal conductivity is 2.383 W/m·K for SLTB3. κ_l is related to lattice distortion [44], a phonon-scattering effect by Bi^{3+} [45] and the average mass of lattice atoms [32]. The larger the lattice distortion is, the smaller the lattice symmetry is. The strain field fluctuation leads to lattice relaxation, which slows down the propagation speed of phonons and inhibits the κ_l [44]. Meanwhile, due to the mass difference between the doped ions Bi^{3+} and Sr^{2+}, the phonon scattering is enhanced, thus reducing the lattice thermal conductivity [45]. However, a lager average mass of lattice atoms lead to higher κ_l [32]. From Table 1, the lattice distortion degree of SLT is larger than SLTB1. Therefore, despite the presence of a phonon-scattering effect by Bi^{3+}, κ_l of SLTB1 increases. When Bi^{3+}-doping concentration increases to 7.4–11.1%, the Ti–O bond length and Bi–O bond length both increase, the lattice distortion degree increases, and the phonon-scattering effect of Bi^{3+} ion increases, so κ_l decreases. κ_l is the lowest when Bi^{3+}-doping concentration is 11.1%. When the Bi^{3+}-doping concentration is further increased to 14.8%, the heavier Bi^{3+} ions greatly increase the average atomic mass of the cell, as shown in Table S2. Despite the enhanced lattice distortion and phonon scattering, the bigger average mass of lattice atoms lead to higher κ_l of SLTB4 than that of SLTB3.

The total thermal conductivity of $(Sr_{0.889\text{-}x}La_{0.111}Bi_x)TiO_{2.963}$ is shown in Figure 8f. The trends of total thermal conductivity and lattice thermal conductivity are basically identical. The total thermal conductivity of SLT, SLTB2, SLTB3, SLTB4 and SLTL is similar except for SLTB1 with a larger total thermal conductivity. Due to the enhanced phonon scattering at high temperature, the total thermal conductivity decreases with increasing temperature,

ranging from 7.4–10.6 W/m·K at room temperature to 2.8–3.9 W/m·K at 1200 K, which is consistent with the reported data of 8.2 W/m·K at 373 K to 2.5 W/m·K at 973 K [36].

Figure 8g shows the *ZT* of $(Sr_{0.889-x}La_{0.111}Bi_x)TiO_{2.963}$ as a function of temperature. The *ZT* of SLTB increases with temperature from 0.06–0.11 (400 K) to 0.25–0.48 (1200 K). The *ZT* of SLT and SLTL increased from 0.09–0.10 (400 K) to 0.37–0.46 (1200 K). When the Bi^{3+} concentration is 7.4%, the maximum *ZT* value is 0.48 for SLTB2 at 1200 K. However, except for SLTB2, the *ZT* values of SLTB are all smaller than that of SLT and SLTL. When the Bi^{3+} concentration is 14.8%, the *ZT* value decreases to 0.25.

The results of thermoelectric calculation show that only an appropriate Bi^{3+}-doping concentration (7.4%) can optimize the thermoelectric properties of materials. A smaller Bi^{3+} concentration (3.7–7.4%) can increase the Seebeck coefficient of the material and thus have a larger power factor, but its thermal conductivity is higher. Although a larger Bi^{3+}-doping concentration (11.1–14.8%) will reduce the thermal conductivity of the material, it will significantly deteriorate the electrical conductivity of the material, resulting in a lower *ZT*. Therefore, the Bi^{3+}-doping concentration could be 7.4%, which is best for practical preparation of the real materials and applications. In the future, more suitable dopants should be searched to improve the electrical transport performance of materials on the basis of reducing the thermal conductivity of materials, so as to obtain excellent thermoelectric performance.

4. Conclusions

The thermoelectric properties of $(Sr_{0.889-x}La_{0.111}Bi_x)TiO_{2.963}$ were studied by the first principles method. The introduction of Bi^{3+} affects the crystal cell structure and electronic structure of $(Sr_{0.889-x}La_{0.111}Bi_x)TiO_{2.963}$, and increases the cell parameters, cell asymmetry and band gap. The introduction of Bi^{3+} increases the asymmetry of DOS with respect to the Fermi level, thus increasing the absolute Seebeck coefficient of the material. When the Bi^{3+} concentration increases, the electronic effective mass increases, the carrier mobility decreases, and the carrier concentration increases. When the Bi^{3+}concentration of is 3.7% and 7.4%, the conductivity and power factor of the material are larger. However, when the Bi^{3+}-doping concentration is higher than 11.1%, the excessive Bi^{3+}-doping concentration greatly deteriorates the electrical conductivity and power factor of the material. The lattice distortion caused by Bi^{3+} doping greatly enhances the phonon scattering and decreases the thermal conductivity. Finally, when Bi^{3+} concentration was 7.4%, the maximum *ZT* of 0.48 for $Sr_{0.815}La_{0.111}Bi_{0.074}TiO_{2.963}$ at 1200 K was obtained. The results show that an appropriate Bi^{3+}-doping concentration (7.4%) can effectively optimize the electrical transport performance of the material, enhance the *ZT* and improve the thermoelectric properties of $SrTiO_3$.

Supplementary Materials: The following supporting information can be downloaded at: https://www.mdpi.com/article/10.3390/cryst13020178/s1, Figure S1: Chemical potential dependent of $S^2\sigma/\tau$ for $(Sr_{0.889-x}La_{0.111}Bi_x)TiO_{2.963}$ at 1200 K; Figure S2: Temperature dependent of τ for $(Sr_{0.889-x}La_{0.111}Bi_x)TiO_{2.963}$; Table S1: Mechanical properties of $(Sr_{0.889-x}La_{0.111}Bi_x)TiO_{2.963}$; Table S2: Thermal properties of $(Sr_{0.889-x}La_{0.111}Bi_x)TiO_{2.963}$.

Author Contributions: Conceptualization, P.Z. and Z.L.; methodology, L.G.; software, L.G.; data curation, P.Z.; writing—original draft preparation, L.G.; writing—review and editing, P.Z. and Z.L.; visualization, Z.W. (Ziyao Wei) and Z.W. (Zhuozhao Wu); supervision, X.C., W.X. and Y.W.; project administration, J.X. and F.G. All authors have read and agreed to the published version of the manuscript.

Funding: This research was funded by National Natural Science Foundation of China (No. 52272123, 52072301), the China-Poland International Collaboration Fund of National Natural Science Foundation of China (No. 51961135301), National Innovative Entrepreneurship Training Program for Undergraduates (S202210699186), the Fundamental Research Funds for the Central Universities (No. D5000210722), the Research Fund of State Key Laboratory of Solidification Processing (NPU)

(No. 2021-TS-08), the Open Fund of State Key Laboratory of New Ceramic and Fine Processing Tsinghua University (No. KFZD202102), and the '111' Project (No. B20028).

Institutional Review Board Statement: Not applicable.

Informed Consent Statement: Not applicable.

Data Availability Statement: The data presented in this study are available on request from the corresponding authors.

Acknowledgments: The authors gratefully acknowledge the National Natural Science Foundation of China, the China-Poland International Collaboration Fund of National Natural Science Foundation of China, National Innovative Entrepreneurship Training Program for Undergraduates, the Fundamental Research Funds for the Central Universi-ties, the Research Fund of State Key Laboratory of Solidification Processing (NPU), the Open Fund of State Key Laboratory of New Ceramic and Fine Pro-cessing Tsinghua University, and the '111' Project.

Conflicts of Interest: The authors declare no conflict of interest.

References

1. Okhay, O.; Zlotnik, S.; Xie, W.; Orlinski, K.; Gallo, M.J.H.; Otero-Irurueta, G.; Fernandes, A.J.S.; Pawlak, D.A.; Weidenkaff, A.; Tkach, A. Thermoelectric performance of Nb-doped SrTiO3 enhanced by reduced graphene oxide and Sr deficiency cooperation. *Carbon* **2019**, *143*, 215–222. [CrossRef]
2. Elsheikh, M.H.; Shnawah, D.A.; Sabri, M.F.M.; Said, S.B.M.; Hassan, M.H.; Bashir, M.B.A.; Mohamad, M. A review on thermoelectric renewable energy: Principle parameters that affect their performance. *Renew. Sust. Energ. Rev.* **2014**, *30*, 337–355. [CrossRef]
3. Zhang, B.; Wang, J.; Zou, T.; Zhang, S.; Yaer, X.; Ding, N.; Liu, C.; Miao, L.; Li, Y.; Wu, Y. High thermoelectric performance of Nb-doped SrTiO3 bulk materials with different doping levels. *J. Mater. Chem. C.* **2015**, *3*, 11406–11411. [CrossRef]
4. Lu, Z.; Zhang, H.; Lei, W.; Sinclair, D.C.; Reaney, I.M. High-figure-of-merit thermoelectric La-doped A site-deficient SrTiO3 ceramics. *Chem. Mater.* **2016**, *28*, 925–935. [CrossRef]
5. Wang, K.X.; Wang, J.; Li, Y.; Zou, T.; Wang, X.H.; Li, J.B.; Cao, Z.; Shi, W.J.; Yaer, X. Enhancement of thermoelectric properties of SrTiO3/LaNb-SrTiO3 composite by different doping levels. *Chin. Phys. B.* **2018**, *27*, 048401. [CrossRef]
6. Li, X.; Zhao, H.; Zhou, X.; Xu, N.; Xie, Z.; Chen, N. Electrical conductivity and structural stability of La-doped SrTiO3 with A-site deficiency as anode materials for solid oxide fuel cells. *Int. J. Hydrogen Energ.* **2010**, *35*, 7913–7918. [CrossRef]
7. Zhang, P.; Gong, L.Y.; Lou, Z.H.; Xu, J.; Cao, S.Y.; Zhu, J.T.; Yan, H.X.; Gao, F. Reduced lattice thermal conductivity of perovskite-type high-entropy (Ca0.25Sr0.25Ba0.25RE0.25)TiO3 ceramics by phonon engineering for thermoelectric applications. *J. Alloys Compd.* **2022**, *898*, 162858. [CrossRef]
8. Qin, M.J.; LouA, Z.H.; Zhang, P.; Shi, Z.M.; Xu, J.; Chen, Y.; Gao, F. Enhancement of thermoelectric performance of Sr0.9La0.1TiO3-based ceramics regulated by nanostructures. *ACS Appl. Mater. Inter.* **2020**, *12*, 53899–53909. [CrossRef]
9. Muta, H.; Kurosaki, K.; Yamanaka, S. Thermoelectric properties of reduced and La-doped single-crystalline SrTiO3. *J. Alloys Compd.* **2005**, *392*, 306–309. [CrossRef]
10. Ohta, S.; Nomura, T.; Ohta, H.; Koumoto, K. High-temperature carrier transport and thermoelectric properties of heavily La- or Nb-doped SrTiO3 single crystals. *J. Appl. Phys.* **2005**, *97*, 034106. [CrossRef]
11. Park, K.; Son, J.S.; Woo, S.I.; Shin, K.; Oh, M.-W.; Park, S.-D.; Hyeon, T. Colloidal synthesis and thermoelectric properties of La-doped SrTiO3 nanoparticles. *J. Mater.* **2014**, *2*, 4217–4224. [CrossRef]
12. Wang, J.; Zhang, B.Y.; Kang, H.J.; Li, Y.; Yaer, X.; Li, J.F.; Tan, Q.; Zhang, S.; Fan, G.H.; Liu, C.Y.; et al. Record high thermoelectric performance in bulk SrTiO3 via nano-scale modulation doping. *Nano Energy* **2017**, *35*, 387–395. [CrossRef]
13. Kinaci, A.; Sevik, C.; Çagin, T. Electronic transport properties of SrTiO3 and its alloys: Sr1-xLaxTiO3 and SrTi1-xMxO3 (M=Nb,Ta). *Phys. Rev. B.* **2010**, *82*, 155114. [CrossRef]
14. Zou, D.; Liu, Y.; Xie, S.; Lin, J.; Li, J. Effect of strain on thermoelectric properties of SrTiO3: First-principles calculations. *Chem. Phys. Lett.* **2013**, *586*, 159–163. [CrossRef]
15. Feng, L.; Shiga, T.; Shiomi, J. Phonon transport in perovskite SrTiO3 from first principles. *Appl. Phys. Express.* **2015**, *8*, 071501. [CrossRef]
16. Gillani, S.S.A.; Ahmad, R.; Din, I.U.; Rizwan, M.; Shakil, M.; Rafique, M.; Murtaza, G.; Jin, H.B. First-principles investigation of structural, electronic, optical and thermal properties of Zinc doped SrTiO3. *Optik* **2020**, *201*, 163481. [CrossRef]
17. Singsoog, K.; Seetawan, T.; Vora-Ud, A.; Thanachayanont, C. Theoretical enhancement of thermoelectric properties of Sr1-xLaxTiO3. *Integr. Ferroelectr.* **2014**, *155*, 111–118. [CrossRef]
18. Li, Y.; Hou, Q.Y.; Wang, X.H.; Kang, H.J.; Yaer, X.; Li, J.B.; Wang, T.M.; Miao, L.; Wang, J. First-principles calculations and high thermoelectric performance of La-Nb doped SrTiO3 ceramics. *J. Mater.* **2019**, *7*, 236–247. [CrossRef]
19. Zhang, R.; Wang, C.; Li, J.; Su, W.; Zhang, J.; Zhao, M.; Liu, J.; Zhang, Y.; Mei, L. Determining Seebeck coefficient of heavily doped La:SrTiO3 from density functional calculations. *Solid State Sci.* **2010**, *12*, 1168–1172. [CrossRef]

20. Baniecki, J.D.; Ishii1, M.; Aso1, H.; Kurihara, K.; Ricinschi, D. Density functional theory and experimental study of the electronic structure and transport properties of La, V, Nb, and Ta doped SrTiO3. *J. Appl. Phys.* **2013**, *113*, 013701. [CrossRef]
21. Adessi, C.; Thébaud, S.; Bouzerar, R.; Bouzerar, G. Ab initio investigation of the role of vanadium impurity states in SrTiO3 for thermoelectricity. *J. Phys. Chem. Solids.* **2020**, *138*, 109180. [CrossRef]
22. Shenoy, U.S.; Bhat, D.K. Electronic structure engineering of SrTiO3 via rhodium doping: A DFT study. *J. Phys. Chem. Solids.* **2021**, *148*, 109708. [CrossRef]
23. Sikam, P.; Sararat, C.; Moontragoon, P.; Kaewmaraya, T.; Maensiri, S. Enhanced thermoelectric properties of N-doped ZnO and SrTiO3: A first principles study. *Appl. Surf. Sci.* **2018**, *446*, 47–58. [CrossRef]
24. Chen, Q.; Zhang, P.; Qin, M.J.; Lou, Z.H.; Gong, L.Y.; Xu, J.; Kong, J.; Yan, H.X.; Gao, F. Effect of La3+, Ag+ and Bi3+ doping on thermoelectric properties of SrTiO3: First-principles investigation. *Ceram. Int.* **2022**, *48*, 13803–13816. [CrossRef]
25. Gong, C.L.; Dong, G.G.; Hu, J.X.; Chen, Y.S.; Qin, M.J.; Yang, S.J.; Gao, F. Effect of reducing annealing on the microstructure and thermoelectric properties of La–Bi co-doped SrTiO3 ceramics. *J. Mater. Sci. Mater. Electron.* **2017**, *28*, 14893–14900. [CrossRef]
26. Zhang, R.Z.; Wang, C.L.; Li, J.C.; Mei, L.M. Theoretical analysis of cascade levels forming in SrTiO3. *Acta Phys. Sin.* **2009**, *58*, 7162–7167. [CrossRef]
27. Qin, M.; Gao, F.; Cizek, J.; Yang, S.; Fan, X.; Zhao, L.; Xu, J.; Dong, G.; Reece, M.; Yan, H. Point defect structure of La-doped SrTiO3 ceramics with colossal permittivity. *Acta Mater.* **2019**, *164*, 76–89. [CrossRef]
28. Tomio, T.; Miki, H.; Tabata, H.; Kawai, T.; Kawai, S. Control of electrical conductivity in laser deposited SrTiO3 thin films with Nb doping. *J. Appl. Phys.* **1994**, *76*, 5886–5890. [CrossRef]
29. Kresse, G.; Furthmüller, J. Efficiency of ab-initio total energy calculation for metals and semiconductors using a plane-wave basis set. *Comput. Mater. Sci.* **1996**, *6*, 15–50. [CrossRef]
30. Wang, V.; Xu, N.; Liu, J.C.; Tang, G.; Geng, W.T. VASPKIT: A user-friendly interface facilitating high-throughput computing and analysis using VASP Code. *Comput. Phys. Commun.* **2021**, *267*, 108033. [CrossRef]
31. Madsen, G.K.H.; Carrete, J.; Verstraete, M.J. BoltzTraP2, a program for interpolating band structures and calculating semi-classical transport coefficients. *Comput. Phys. Commun.* **2018**, *231*, 140–145. [CrossRef]
32. Slack, G.A. Nonmetallic crystals with high thermal conductivity. *J. Phys. Chem. Solids.* **1973**, *34*, 321–335. [CrossRef]
33. Bardeen, J.; Shockley, W. Deformation potentials and mobilities in non-polar crystals. *Phys. Rev.* **1950**, *80*, 72–80. [CrossRef]
34. Kohn, W.; Sham, L.J. Self-consistent equations including exchange and correlation Effects. *Phys. Rev. A.* **1965**, *140*, A1133. [CrossRef]
35. Hashimoto, S.; Kindermann, L.; Poulsen, F.W.; Mogensen, M. A study on the structural and electrical properties of lanthanum-doped strontium titanate prepared in air. *J. Alloy. Compd.* **2005**, *397*, 245–249. [CrossRef]
36. Chen, C.; Bousnina, M.; Giovannelli, F.; Delorme, F. Influence of Bi on the thermoelectric properties of SrTiO3-δ. *J. Materiomics* **2019**, *5*, 88–93. [CrossRef]
37. Benrekia, A.R.; Benkhettou, N.; Nassour, A.; Driz, M.; Sahnoun, M.; Lebèguec, S. Structural, electronic and optical properties of cubic SrTiO3 and KTaO3: Ab initio and GW calculations. *Physica. B Condens.* **2012**, *407*, 2632–2636. [CrossRef]
38. Benthem, K.V.; Elsässer, C.; French, R.H. Bulk electronic structure of SrTiO3: Experiment and theory. *J. Appl. Phys.* **2001**, *90*, 6156. [CrossRef]
39. Zilber, T.; Cohen, S.; Fuks, D.; Gelbstein, Y. TiNiSn half-Heusler crystals grown from metallic flux for thermoelectric applications. *J. Alloys Compd.* **2019**, *781*, 1132–1138. [CrossRef]
40. Vurgaftman, I.; Meyer, J.R.; Ram-Mohan, L. Band parameters for III–V compound semiconductors and their alloys. *J. Appl. Phys.* **2001**, *89*, 5815–5875. [CrossRef]
41. Wang, N.; Li, M.; Xiao, H.; Gong, H.; Liu, Z.; Zua, X.; Qiao, L. Optimizing the thermoelectric transport properties of Bi2O2Se monolayer via biaxial strain. *Phys. Chem. Chem. Phys.* **2019**, *21*, 15097–15105. [CrossRef] [PubMed]
42. Ganguly, P.; Vasanthacharya, N.Y.; Rao, C.N.R.; Edwards, P.P. Composition-controlled metal-insulator transitions and minimum metallic conductivity in the oxide systems LaNi1-xMxO3 (M = Cr, Mn, Fe, or Co). *Phys. Rev. B Solid State* **1978**, *17*, 2575–2581. [CrossRef]
43. Sun, J.F.; Singh, D.J. Thermoelectric properties of n-type SrTiO3. *APL Mater.* **2016**, *4*, 104803. [CrossRef]
44. Wan, C.L.; Pan, W.; Xu, Q.; Qin, Y.X.; Wang, J.D.; Qu, Z.X.; Fang, M.H. Effect of point defects on the thermal transport properties of (LaxGd1−x)2Zr2O7 experiment and theoretical model. *Phys. Rev. B.* **2006**, *74*, 144109. [CrossRef]
45. Liu, D.; Zhang, Y.; Kang, H.; Li, J.L.; Chen, Z.N.; Wang, T.M. Direct preparation of La-doped SrTiO3 thermoelectric materials by mechanical alloying with carbon burial sintering. *J. Eur. Ceram. Soc.* **2018**, *38*, 807–811. [CrossRef]

Disclaimer/Publisher's Note: The statements, opinions and data contained in all publications are solely those of the individual author(s) and contributor(s) and not of MDPI and/or the editor(s). MDPI and/or the editor(s) disclaim responsibility for any injury to people or property resulting from any ideas, methods, instructions or products referred to in the content.